Parameters Influencing the Characteristic Exhaust Velocity of a N_2O/C_2H_4 Green Propellant

Lukas Werling * and Patrick Bätz †
German Aerospace Center (DLR), Lampoldshausen, Germany, 74239

Currently several green propellants are under investigation to replace the toxic and carcinogenic monopropellant hydrazine (N_2H_4). Beside alternatives as Ammonium dinitramide (ADN)-based propellants, Hydroxylammonium nitrate (HAN)-based mixtures or high concentrated hydrogen peroxide (H_2O_2), mixtures of fuels with nitrous oxide - called HyNOx or NOFBX represent promising green propellants. Compared to classical hydrazine, N_2O/fuel mixtures offer a higher performance (I_{sp}, c^*), no or low toxicity and low propellant costs. To investigate the handling and performance of a propellant mixture consisting of nitrous oxide (N_2O) and ethene (C_2H_4), hot gas combustion tests with an experimental combustor were conducted. This paper summarizes the results of 134 combustion tests conducted with the premixed propellant injected in gaseous state. Calculated and measured performance (c^* and η_{c^*}) depending on mixture ratio, characteristic combustion chamber length (L^*) and chamber pressure are shown and discussed. Furthermore the residence time scales of the propellant mixture inside the combustion chamber are normalized by the chemical time scale of the combustion process. Thus combustion efficiencies depending on dimensionless Damköhler numbers are derived.

Nomenclature

A_{cc} = Cross sectional area of combustion chamber, m^2

A_e = Cross sectional area of nozzle exit, m^2

A_t = Nozzle throat area, m^2

α = Thermal diffusivity, $\frac{m^2}{s}$

c^* = Characteristic exhaust velocity, $\frac{m}{s}$

c^*_{exp} = Experimentally derived c^*, $\frac{m}{s}$

c^*_{theo} = Theoretical c^*, $\frac{m}{s}$

c_p = Specific heat at constant pressure, $\frac{J}{kg \cdot K}$

*Head Facilities Group/M11 Test Facility, Satellite and Orbital Propulsion Department, Im Langen Grund, D-74239 Hardthausen, Germany, AIAA Member

†Master Thesis Student, Satellite and Orbital Propulsion Department, Im Langen Grund, D-74239 Hardthausen, Germany

Da = Damköhler number $\left(\frac{\tau_{res}}{\tau_{chem}}\right)$

d_t = Nozzle throat diameter, m

η_{c^*} = c^* or combustion efficiency $\left(\frac{c^*_{exp}}{c^*_{theo}}\right)$

ϵ = Expansion ratio $\left(\frac{A_e}{A_t}\right)$

ϵ_c = Contraction ratio $\left(\frac{A_e}{A_t}\right)$

I_{sp} = Specific impulse, s

κ = Ratio of specific heats

λ = Thermal conductivity of the propellant, $\frac{W}{m \cdot K}$

L^* = Characteristic combustion chamber length, m

L_{cc} = Combustion chamber length (injector to nozzle throat), m

L^*_{opt} = Smallest characteristic combustion chamber length at which a maximum of c^* is obtained, m

$\dot{m}$ = Propellant mass flow rate, $\frac{kg}{s}$

ROF = Propellant mass mixture ratio (oxidizer to fuel)

p_{cc} = Combustion chamber pressure, bar

ρ = Density of burned gas in the combustion chamber, $\frac{kg}{m^3}$

ρ_u = Density of unburned gas in the combustion chamber, $\frac{kg}{m^3}$

S_L = Laminar flame speed, $\frac{m}{s}$

τ_{chem} = Chemical time scale, s

τ_{flow} = Average flow time of the burned gases to pass the combustion chamber, s

τ_{res} = Residence time of the unburned gas to pass the combustion chamber, s

T_{cc} = Temperature in the combustion chamber, K

V_{cc} = Volume of the combustion chamber, m^3

I. Introduction

Since the early days of spaceflight hydrazine (N_2H_4) is used as a monopropellant to power rockets, satellites or probes [1, 2]. During the 1950s and 1960s a large number of different propellants were tested to be used as a monopropellant [3]. Among these propellants, hydrazine proved to be the best choice. N_2H_4 offered a sufficient performance, long term storability, handling with a very low risk of explosions and relatively low costs. These characteristics made hydrazine the commonly used monopropellant to the present day. Additionally space flight and the operation of satellites are a business which is strongly focused on reliability. Thus development and qualifications of new propellants and thrusters consume lots of time and money. However, during the last decade the high toxicity of hydrazine became a growing point of concern. In the EU the so-called REACH (Registration Evaluation Authorization and Restriction

of Chemicals)-Regulation came into effect and hydrazine was included in the list of substances of very high concern (SVHC). Thus it becomes more and more likely that the use of hydrazine will be limited or prohibited in future, even though exceptions for the space industry might be given. To compensate a possible prohibition of hydrazine several so-called green propellants are under development or qualification. Among those alternatives, the ADN-based monopropellant LMP-103S is the most developed substance for orbital propulsion. In 2010 the evaluation of LMP-103S started in space with two 1 N ADN-thrusters on board the PRISMA satellite project while up to now 13 SkySat satellites of Planet [4] are in orbit and equipped with an LMP-based propulsion systems. Nevertheless other propellants or propellant mixtures than LMP-103S offer advantages compared to conventional hydrazine and are therefore under thorough investigations. Recently, also the HAN-based propellant AFM-315E or ASCENT was tested aboard the GPIM mission [5]. The following chapter will give a short overview of some alternatives. The green propellant focused on in this paper is a mixture of nitrous oxide and ethene. Those propellants are called Nitrous Oxide Fuel Blends (NOFB) or Hydrocarbons mixed with Nitrous Oxide (HyNOx).

This paper summarizes the results of an extended test campaign with a N_2O/C_2H_4 green propellant mixture. The aim of the campaign was to evaluate the performance of the propellant depending on the mixture ratio, chamber pressure and characteristic combustion chamber length. First, the test should experimentally confirm the calculated propellant performance and confirm the potential of the mixture to replace hydrazine. Second, the influence of the characteristic chamber length L^* on the characteristic exhaust velocity and combustion efficiency is investigated. By knowing the characteristic chamber length, future combustion chambers and thruster can be designed efficiently. Third, the influence of the mixture ratio and chamber pressure on the characteristic exhaust velocity is examined. The analysis of the mixture ratio and chamber pressure will give boundary conditions for the efficient operation of future thrusters and propulsion systems. Finally, the connections found between the mentioned parameters for the N_2O/C_2H_4 propellant might also be transferable to other propellants or propellant combinations.

A. Green propellants overview

The following section gives a short overview of the currently investigated green propellant alternatives which could replace the monopropellant hydrazine. Due to the wide range of research activities concerning green propellants or green propellant combinations, the paragraph makes no claim to completeness. An overview and details of all currently investigated green monopropellants can be found in [6]

1. Ammonium dinitramide (ADN)-based propellants

ADN-based monopropellants mainly consist of ammonium dinitramide, a fuel, water and a stabilizer. As ADN is an ionic liquid, those propellants or propellant mixtures are also called energetic ionic liquids. The most known ADN-based propellants are LMP 103S, invented by the Swedish company ECAPS and FLP-106, developed by FOI

(Swedish Defense Research Agency). LMP-103S offers a 6%-8% higher specific impulse (253 s) than hydrazine and a 24% higher density while being less toxic and not carcinogenic [4, 7, 8]. The storability of LMP-103S was already tested for more than 7 years and the propellant can be ignited by using a preheated catalyst (approx. 340-360°C) [4]. FLP-106 offers an even higher specific impulse (about 260 s) caused by higher combustion temperatures [8]. The main difference of FLP-106 in comparison to LMP-103S is the usage of a less volatile fuel. Detailed information about ADN-based monopropellants can be found in references [4, 7–9].

2. Hydroxylammonium nitrate (HAN)-based propellants

HAN (hydroxylammonium nitrate)-based propellants are another class of energetic ionic liquids. Those propellants were intensively investigated since the 1960s to be used as liquid gun propellant. Finally, during the 1980s the liquid gun propellant LP1846 was developed [10]. Caused by the search for high performance alternatives to hydrazine, HAN-based propellants got into the focus of research. The research activities lead to the development of the HAN based propellant AF-M315E [11] and the propellant formulation SHP 163 [12–14]. AF-M315E was selected for the Green Propellant Infusion Mission (GPIM) [11] and is currently tested in orbit. AF-M315E may offer an I_{sp} of 248 s and a 46% higher density than hydrazine [11]. The thrusters are ignited by a preheated catalyst. As the combustion temperature of AF-M315E exceeds the combustion temperature of conventional hydrazine, high temperature catalysts and chamber materials are needed.

3. High concentrated hydrogen peroxide H_2O_2

Hydrogen peroxide is another, well studied green propellant alternative. The main advantages of H_2O_2 are a negligible toxicity, easy ignitability via catalyst, relatively low decomposition temperatures (up to 1230 K) and a high density (1440 kg/m^3) [15]. The drawbacks of H_2O_2 are a lower I_{sp} than hydrazine (up to 185 s [16], depending on concentration), the incompatibility with numerous materials (e.g. copper, iron, magnesium alloys, titanium) and the corresponding slow decomposition processes [17]. Due to the good availability of high concentrated hydrogen peroxide, well studied catalysts and decades of experience in handling the substance, hydrogen peroxide seems to be a very promising alternative for several monopropellant applications [18, 19]. A further advantage of hydrogen peroxide is, that it can also be used as oxidizer in hypergolic bipropellant combinations [20].

4. Water electrolysis propulsion

Another possible – definitely non-toxic and green - alternative to hydrazine is water electrolysis propulsion [21, 22]. Here the idea is to fuel a satellite with water and decompose the water in orbit via an electrolyzer into hydrogen and oxygen. The gaseous hydrogen and oxygen are then stored in separate tanks. When enough H_2 and O_2 was produced, the gases are taken from the tanks and burned in a satellite thruster at a low mixture ratio to assure modest combustion

temperatures. Remaining oxygen can be used in a cold gas propulsion system or added to the air of a manned space station [23]. Ignition of the H_2/O_2 is achieved by using a platinum catalyst. Easy handling of the purified water, no safety and toxicity concerns and available technologies (electrolyzers) are the main advantages of water electrolysis propulsion. Drawbacks are a quite complex propulsion system with three tanks, necessary pressure regulators, valves, bipropellant injectors and a corresponding high weight of the whole propulsion system. Additionally the avoidance of H_2 leakage in a later propulsion system might be challenging.

5. Nitrous oxide fuels blends (NOFBX) or mixtures of hydrocarbons with nitrous oxide (HyNOx)

Another type of prospective, low cost and high performance propellants are mixtures of nitrous oxide (N_2O) and fuels, also known as nitrous oxide fuel blends [24, 25]. Those propellants are no single species monopropellants, but mixtures of the oxidizer (N_2O) and one or more fuels (e.g. C_2H_2, C_2H_4, C_2H_6 or C_2H_5OH). Nitrous oxide/fuel propellants are stored premixed and liquefied, i.e. monopropellant-like in one tank. In comparison to a classical bipropellant system, only a single tank, feeding line and injection system is needed. Thus these propellants are sometimes called "premixed monopropellants", offering a monopropellant like system while having a bipropellant performance (I_{sp} up to 325 s [24]). The high vapor pressure of the mixtures (up to 5 MPa at 20°C) allow a self-pressurized propulsion system without any external pressure supply. Beside the mentioned advantages, nitrous oxide fuel blends provide some non-minor challenges: Very high combustion temperatures (> 3000 K) require an active cooling of the nozzle and combustion chamber. Furthermore the propulsion system needs proper flashback arresters and newly designed ignition and injection systems [26, 27]. If a flame flashback or an unwanted ignition occurs, the flame could propagate into the propellant tank and destroy the entire spacecraft. The most known nitrous oxide fuel blend is NOFBX from Firestar/ISPS [24]. Furthermore investigations on a nitrous oxide/acetylene propellant mixture called NA-7 were carried out. During a test campaign with this propellant two explosions occurred [28].

In the frame of the research activities described in this paper, a dinitrogen monoxide/ethene propellant mixture was chosen for investigation [25, 29, 30]. Ethene was selected as fuel due to a similar vapor pressure to nitrous oxide (vapor pressure at 273 K: C_2H_4: 41 bar; N_2O: 31.2 bar [31]). The similarity concerning the vapor pressures should assure good miscibility and simultaneous evaporation in a propellant tank. Furthermore ethene is quite safe to handle, so compared to acetylene self-decomposition hazards can be avoided. Though the theoretical vacuum specific impulse is lower in comparison to a mixture of nitrous oxide and acetylene (approx. 305 s for $N_2O\&C_2H_4$ compared to 315 s for $N_2O\&C_2H_2$ for an expansion ratio of 50 and a frozen flow in the supersonic part of the nozzle [16]). To gain experience with the propellant mixture and to conduct first combustion tests, the oxidizer and fuel were mixed in their gaseous state upstream the injector of a rocket combustor. The use of the gaseous oxidizer and fuel offers several advantages: 1) the mixture ratio and mass flow can be adjusted easily via exchange of orifices and/or adjusting the feeding line pressure, 2) common gas bottles can directly be connected to the setup, 3) easy comparability to CFD simulations is possible;

no evaporation effects of the liquefied propellant have to be considered, 4) if a hard ignition or a flashback across the injector occurs, due to lower density and propellant mass in the feeding lines less damage will be caused.

Table 1 summarizes all mentioned green propellant alternatives and compares their characteristics to hydrazine.

Table 1 Selected properties of green propellant alternatives to hydrazine

	Propellant						
Property	Hydrazine	LMP-103S	FLP-106	AF-M315E	H_2O_2	Water Propulsion	NOFBX/ HyNOx
Max. vac. I_{sp} [s]	230-245 [2]	252-253 [8]	258-261 [2, 8]	248-250 [2, 11]	185 [8]	300 [16]	300-325
Comb./decomp. temperature [K]	1423 [8]	1903 [32]	2183 [8]	≈ 2000	1230 [16]	1700 O/F=1,5 [16]	3000-3473 [16, 24]
Liquid density [kg/m^3]	1000 [2]	1238 [8]	1357 [8]	1470 [2]	1440 [2]	1000	≈800 [31]
Toxicity	High	Low	Low	Low	Very low	Very low	Very low
System complexity	Low	Low	Low	Low	Low	High	Medium
Storability	Good	Good	Good	Good	Medium	Good	Good
TRL	Very high	High	Low	Medium	High	Low	Low

II. Rocket Combustor Performance

To evaluate the performance of a rocket propellant, the characteristic exhaust velocity c^* is a commonly used parameter. By comparing the experimental c^* (c^*_{exp}) to the theoretical c^* (c^*_{theo}), the c^*-efficiency (η_{c^*}) can be derived. The specific impulse I_{sp} is a widely used parameter to analyze the overall system performance and to take nozzle effects into account. Compared to the specific impulse I_{sp}, the characteristic velocity c^* is mainly a function of the burned propellant, the mixture ratio, the chamber pressure as well as the injector and the combustion chamber design and is independent of the nozzle characteristic. So by means of c^* different propellant combinations and combustion chamber designs can be compared to each other [1, 33]. Reduced c^*_{exp} and a corresponding reduced η_{c^*} show losses in the combustion chamber caused by a) heat fluxes, b) chemical non-equilibrium, c) non-ideal mixing, d) mixture variations, e) incomplete reactions as well as losses caused by f) boundary layers or g) non-uniformity of the overall flow field. To derive the experimental c^*_{exp} from test data, equation 1 is used:

$$\mathbf{c^*_{exp}} = \frac{\mathbf{p_{cc}\, A_t}}{\mathbf{m}} \tag{1}$$

p_{cc} represents the stagnation pressure in the combustion chamber, A_t is the nozzle throat area and $\dot{m}$ the propellant mass flow. For the later analysis, the experimentally obtained c^*_{exp} was compared to theoretical c^*_{theo} to calculate the combustion efficiency η_{c^*} of the corresponding test. The theoretical c^*_{theo} for the given mixture ratio and pressure was

obtained via CEA [16] computer code. The c^*-efficiency was calculated via equation 2:

$$\eta_{c^*} = \frac{c^*_{exp}}{c^*_{theo}} \tag{2}$$

The experimentally obtained c^*_{exp} values and the division by the theoretical c^*_{theo} values indicate the combustion efficiency. The characteristic combustion chamber length L^* is further design parameter for rocket combustion chambers. L^* is defined as the chamber volume V_{cc} divided by the nozzle throat area A_t:

$$L^* = \frac{V_{cc}}{A_t} \approx \frac{L_{cc}\, A_{cc}}{A_t} \tag{3}$$

Neglecting the volume of the diverging nozzle part and the injector faceplate, the overall volume V_{cc} of a cylindrical combustion chamber corresponds to the chamber length L_{cc} multiplied by the chambers cross sectional area A_{cc}. The optimum L^*_{opt} for a given chamber geometry, injection system and propellant combination is achieved, if c^* and the corresponding combustion efficiency η_{c^*} reaches a maximum.

Assuming a constant density across the combustor, the combustion chamber volume V_{cc} can be rewritten as:

$$V_{cc} = \frac{\dot{m}\, \tau_{flow}}{\rho} \tag{4}$$

Where $\dot{m}$ is the propellant mass flow rate, τ_{flow} the time the propellant needs to pass the combustion chamber and ρ is the average density of the gas in the combustion chamber. Inserting equation 4 in equation 3 gives:

$$L^* = \frac{\dot{m}\, \tau_{flow}}{\rho\, A_t} \tag{5}$$

A. Experimental analysis of c^*

For a given propellant, five general factors are influencing the characteristic exhaust velocity and the combustion efficiency:

1) The chamber pressure p_{cc}. With rising chamber pressure, the chemical time scale of the reaction decreases. A smaller chemical time scale leads to faster reactions and shifts the reactions to the ideal "infinite fast" combustion process. Furthermore the combustion temperature rises with increasing pressure and the chemical composition of the exhaust gases changes.

2) The oxidizer to fuel mixture ratio. The mixture ratio influences the exhaust gas composition as well as the combustion temperature and thus influences the obtained c^*.

3) The residence time of the flow. The oxidizer and fuel can burn completely if the available time for the reacting propellant is sufficiently high. Enough time must be available to assure proper atomization, vaporization, mixing and

combustion or decomposition of the propellant. A too short residence time in the combustion chamber results in unburned oxidizer and fuel. Otherwise if the residence time/flow time scale is too large, the combusted gases lose heat to the combustion chamber walls.

4) The chamber surface area. The surface area of the combustion chamber determines how much heat is conducted from the combusting gases to the chamber walls. An increase in surface area will lead to higher absolute heat losses. A decrease in surface area or a regenerative cooling system will diminish the energy losses. Furthermore a large volume to surface area ratio minimizes the surface available for heat losses.

5) The atomization, vaporization and - in the case of bipropellants - the mixing processes of oxidizer and fuel. The propellant needs to be fully atomized, vaporized and mixed to assure a complete combustion and a high combustion efficiency. These three processes are strongly influenced by the injector design. The injector furthermore determines how much turbulence is generated during the injection process. Turbulences can amplify the atomization, vaporization and mixing processes and thus increase the burn rate and c^*.

To analyze the effect of a single factor during a test campaign, the other influencing parameters should be kept constant, while the investigated parameter is varied. In the reality of an experimental combustion test, this is really hard if not impossible. This comes clear if the residence time, mixture ratio and pressure should be kept constant while the chamber surface has to be changed. This would only be possible by a very precise adjustment of the nozzle throat diameter and the mass flow – otherwise the residence time scale would change with the combustion chamber length or surface.

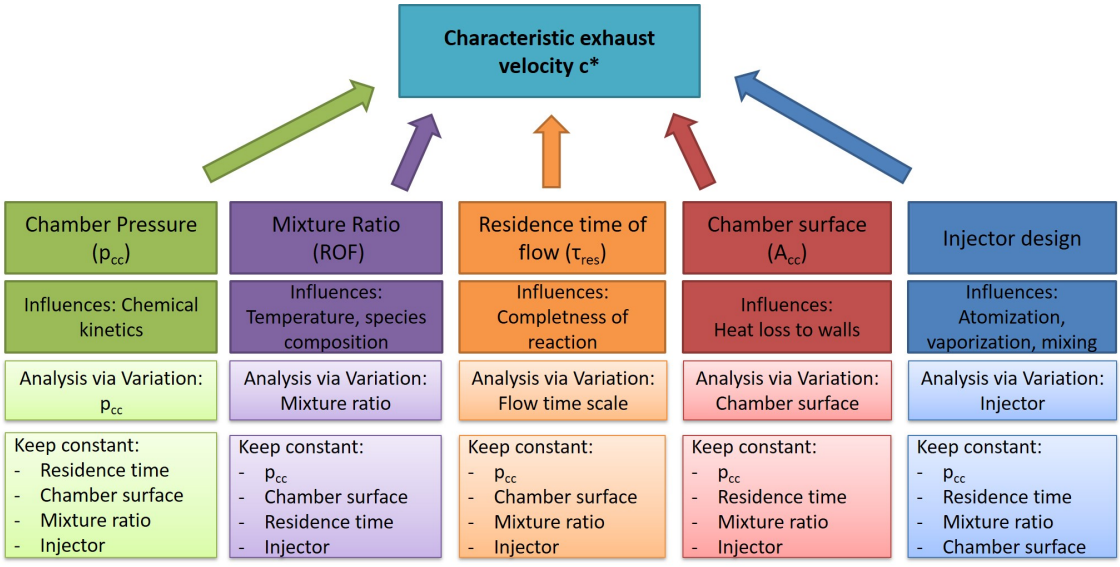

Fig. 1 Parameters influencing c^* and possible analysis of the corresponding parameter

Additionally the mentioned parameters are not independent from each other, e.g. the chamber pressure affects the heat flux to the chamber walls [34]. Figure 1 gives an overview on the influencing parameters on c^* and the methods to

analyze the corresponding effects.

Figure 2 shows the mentioned factors and their assumed effect on c^* for a given, fixed injector design. The characteristic combustion chamber length L^* combines two of the four parameters shown in figure 2: The flow time scale τ_{flow} and the chamber surface area A_{cc}. First the nozzle throat area in the equation of L^* (equation 3) determines the flow speed and therefore the residence time of the gases in the combustion chamber. Second the volume (and the shape) of the combustion chamber determines the wall surface area of the chamber and influences also the residence time/flow time scale. Taking the aforementioned effects into account the optimum L^*_{opt} is connected to the time scale of the reaction and to the average flow time of the propellant inside the combustion chamber. An optimum L^*_{opt} is reached if the chemical energy of the reactants involved is completely converted into heat and pressure as well as the energy losses caused by the interaction with the chamber walls are at a minimum. The propellant should stay just as long in the combustion chamber to react sufficiently. Energy losses to the chamber walls can be reduced by a smaller chamber surface area or for a given chamber surface area by using a regenerative cooling system.

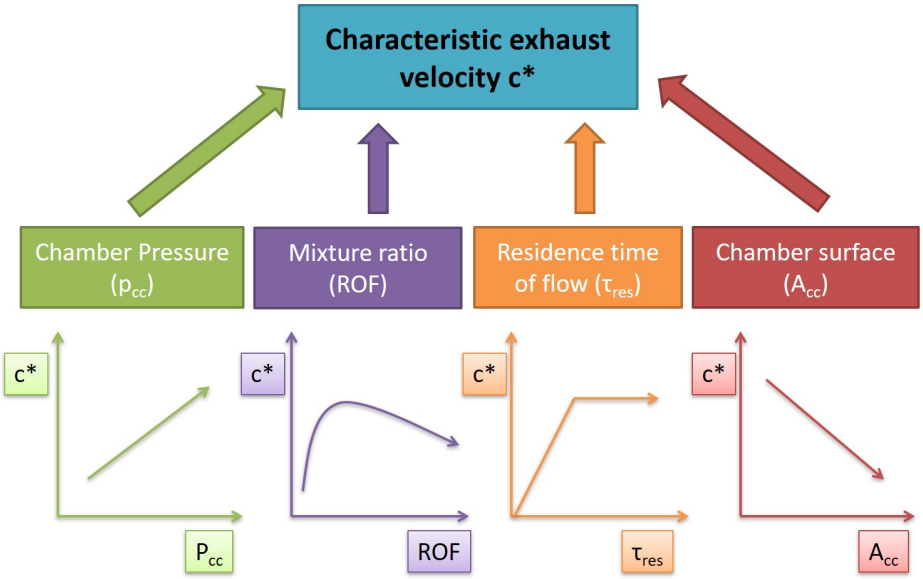

Fig. 2 Parameters influencing c^* and their assumed effect on the characteristic exhaust velocity

III. Test Setup and Experimental Procedure

A simplified sketch of the test bench's fluid system is shown in figure 3. Nitrous oxide (N_2O, grade 2.5 = 99.5 %) and ethene (C_2H_4, grade 3.0 = 99.9 %) are stored in 50 liter gas bottles outside the test bench. The gas bottles are not equipped with a riser pipe, thus the fuel and oxidizer were taken in gaseous phase from the top of the bottles. The feeding line pressure, mixture ratio and the resulting mass flow are adjusted via pressure regulators and calibrated orifices. To purge the combustor, to realize redline shutdown sequences and for operation of the pneumatic valves a nitrogen supply is used. The mass flow of the oxidizer and fuel are measured via coriolis mass flow meters (Emerson CMF025

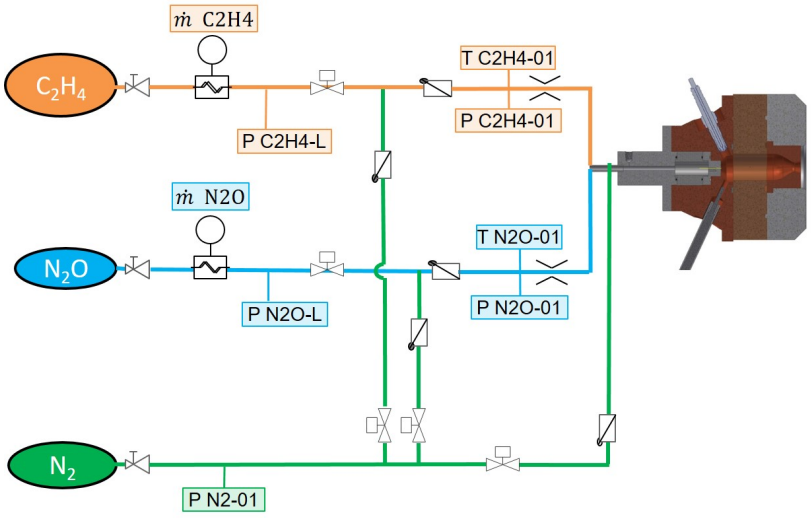

Fig. 3 Schematic P&ID of the test bench

and Rheonik RHM015). The oxidizer and fuel feeding lines are equipped with two pressure transducers (Schaevitz P913) each: One upstream the main valve to check the feeding pressure and a second one in front of the orifices. Additionally type K-thermocouples are mounted upstream the orifices. The data acquisition rate for the pressure sensors is 5 kHz while the thermocouples and the coriolis data are recorded with 100 Hz and 10 Hz, respectively. During the test campaign the oxidizer and fuel are mixed in their gaseous state approximately 0.2 m upstream the injector of the combustor. The mixing tales place at a tee where the fuel and oxidizer tubes are connected. The mixing of gaseous oxidizer and fuel is assumed quite good, as in case of flame flashbacks the tube immediately downstream of the tee connector starts to burn [35].

A. Experimental Combustion Chamber

A sectional view of the capacitively cooled (heat-sink) combustor is presented in figure 4a, a drawing of the injector can be found in figure 5. The connection to the feeding lines is shown on the left hand side of figure 4a.

The gaseous propellant mixture passes the showerhead injector (16 bores with 0.65 mm) and is ignited via spark or glow plug. The front and sectional view of the injector is shown in figure 5, the bores have a length of 2 mm, what results in a length/diameter ratio of approximately 3. Depending on the wanted chamber length, a different number of chamber segments with different lengths could be mounted. The segments, the injector fitting and the nozzle consist of CuCr1Zr and are not actively cooled. Each segment is equipped with three type-K thermocouples in different distances (3 mm, 8 mm and 13 mm) to the inner chamber wall and a pressure transducer (Schaevitz 913 or Kistler 4043). In further investigations [36–38] the thermocouple's data were used to derive the average and transient heat flux to the chamber walls. The inner diameter of the combustion chamber is 0.024 m.

The chamber segments are available in different axial lengths, thus a wider range of chamber sizes can be achieved via

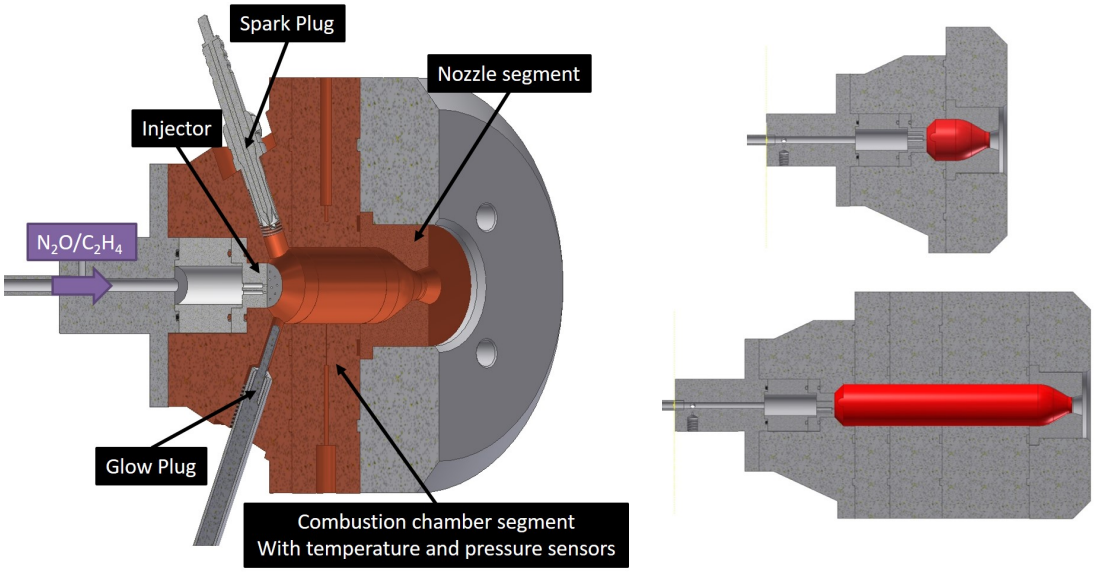

(a) Sectional view of the used combustor

(b) Two different chamber configurations with L_{cc}=0.0305 m (top) and L_{cc}=0.1405 m (bottom)

Fig. 4 Used combustor and different chamber lengths

combining shorter and longer parts. On the right hand side of figure 4a the nozzle segment is shown. During the test campaign, convergent-divergent nozzles with throat diameters of 5 to 9 mm were used. All nozzles have an expansion ratio (ϵ) of 1.75 and all tests were conducted under atmospheric conditions. Table 2 gives an overview on the possible chamber length and nozzle combinations and the resulting L*. Additionally figure 4b illustrates two different chamber lengths.

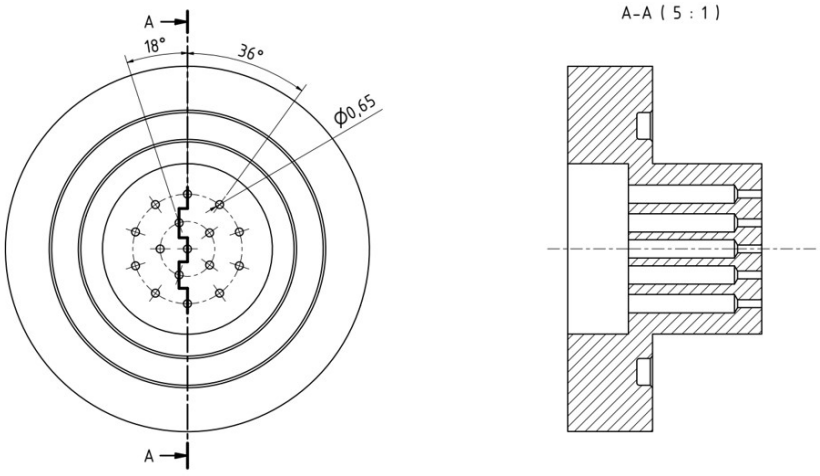

Fig. 5 Front and side view of the showerhead injector with 16 bores of 0.65 mm diameter

Table 2 Chamber length/nozzle combinations and resulting L^*

		Nozzle throat diameter [mm]					
		5	6	7	8	9	
Combustion chamber length L_{cc} [m]	0.0305	0.56	0.39	0.29	0.23	0.18	Resulting L^* [m]
	0.0405	0.79	0.55	0.41	0.32	0.26	
	0.0455	0.90	0.63	0.47	0.36	0.29	
	0.0505	1.02	0.71	0.53	0.41	0.33	
	0.0555	1.13	0.79	0.59	0.45	0.36	
	0.0605	1.25	0.87	0.65	0.50	0.40	
	0.0655	1.36	0.95	0.71	0.54	0.43	
	0.0705	1.48	1.03	0.76	0.59	0.47	
	0.0755	1.59	1.11	0.82	0.63	0.50	
	0.0805	1.71	1.19	0.88	0.68	0.54	
	0.1105	2.40	1.67	1.23	0.95	0.75	
	0.1405	3.09	2.15	1.59	1.22	0.97	

B. Test Procedure

Prior to the each test day, the combustion chamber and the whole setup were leak tested. At the beginning of a test sequence, the mixture ratio and pressure were adjusted manually via pressure regulators. During a cold flow the approximate mass flow and the propellant mixture ratio was checked and corrected if not in the desired range.

Subsequent to the cold flows, the automatic test sequence was started. The setup was purged with nitrogen for 3 s, followed by 10 s of waiting to release the nitrogen. Then the spark or glow plug was activated and the N_2O and C_2H_4 valves were opened. The test duration was 10 s to assure a steady state combustion and to obtain a sufficient time span to evaluate the chamber pressure and the mass flow.

After 10 s the N_2O and C_2H_4 valves were closed. If the chamber's wall temperature was higher than 150°C the combustion chamber was cooled via nitrogen purge until the temperature of the segments fell below 150°C.

Each test was repeated twice with nearly identical mass flow and mixture ratio – slight variations in the mixture ratio and mass flow were caused by small differences of the supply pressure and/or temperature in between two test runs. Typically the difference of the overall mass flow in between the test run and its repetition was below 0.1 g/s while the mixture ratio (ROF) variation was below 0.2.

C. Measurement Error

To calculate the measurement error and derive the error bars, the deviation of each pressure and temperature sensor was analysed via end to end comparison to calibrated devices (Beamex MC5). The maximum deviation of the Coriolis mass flow sensors were obtained from the manufacturers data sheet. After deriving the sensor's deviation, equation 6 from [39] was used to calculated the error propagation of the pressure, the mixture ratio and of the experimental c^*.

$$u_y = \sqrt{\left(\frac{\partial y}{\partial x_1} u_1\right)^2 + \left(\frac{\partial y}{\partial x_2} u_2\right)^2 + \ldots} \tag{6}$$

In equation 6, u_y marks the overall deviation, depending on the derivative of equation y (in our case c^*) to the single variables x_1, x_2, etc. here p_{cc}, d_t, $\dot{m}$. According to the manufacturers data sheet, the maximum error of the Coriolis mass flow sensor (Emerson CMF025 and Rheonik RHM015) were determined to 1.44 %. This deviation occurs only when the mass flow is at the far end of the measurement range. Due to the error of the mass flow sensor, the mixture ratio's deviation was derived correspondingly. The pressure sensors of the combustion chamber were pressurized in parallel with a calibration module (Beamex MC5). The resulting data recorded by the measurement system was compared to the measured values by the calibration module. As result of this end to end comparison a maximum sensor deviation of +/- 0.8 % was observed. The nozzle's throat diameters were measured by a calibrated micrometer under ambient temperatures before each test run and in hot conditions after the test runs. Due to heating of the nozzle segment the throat diameter varied by a maximum of + 0.012 mm. For the calculation of c^*, the actually measured nozzle throat diameter was taken into account.

Nozzle throat diameter [mm]	5	6	7	8	9
Contraction ratio (ϵ_c)	23.09	15.93	11.74	9.00	7.11

Table 3 Nozzle throat diameter and resulting contraction ratio

The contraction ratios of the used chamber/nozzle combinations are shown in Table 3. Due to quite high contraction ratios (ϵ_c), only low Mach numbers (Ma < 0.08) occur in the combustion chamber. Nevertheless, for each test run the measured static pressure was corrected to obtain the corresponding stagnation pressure.

IV. Test Results and Discussion

During several test series the combustion chamber length, the mixture ratio, the nozzle throat diameter and the mass flow rate was varied. In total 134 combustion tests were conducted. A snapshot of one of the conducted combustion tests is shown in figure 6a. Figure 6b gives an example of the pressure data vs. the test time during a test run with ROF=6.7, $\dot{m}$=9.9 g/s.

The black and green lines in figure 6b indicate the N_2O and C_2H_4 feeding line pressures, while the red line marks the chamber pressure. At the beginning of the test sequence (t = -13 s to -10 s) the purging of the feeding lines with N_2 is visible. Ignition takes place at t = 0 s when the N_2O and C_2H_4 valves are opened and the spark plug is activated. The duration of the hot run in figure 6b is 11 s (10 s test time + 1 s ignition sequence). The chamber pressure during the combustion process reaches 7.8 bar and due to the premixed, gaseous state of the propellant no pressure oscillations are visible. After closing the N_2O and C_2H_6 supply, the combustor and feeding lines are purged with N_2 again (starting at t

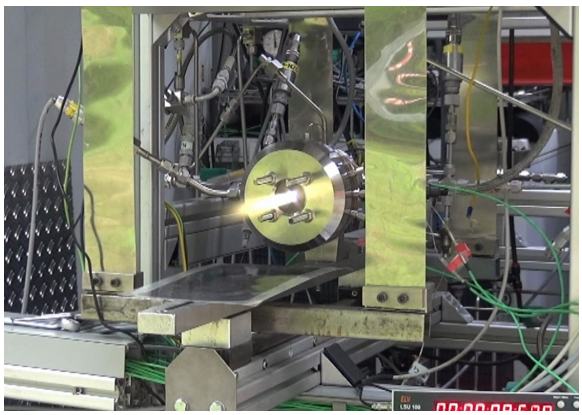

(a) Hot run of the HyNOx combustor

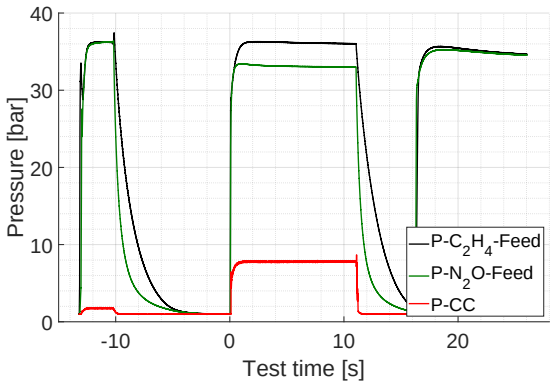

(b) Typical pressure data of a hot run, $\dot{m}$=9.9 g/s, ROF=6.7

Fig. 6 Photo and pressure data of a typical test run

= 16 s). The large pressure drop of the feeding lines (33 bar - 8 bar =) 25 bar, respectively (36 bar - 8 bar) = 28 bar are caused by the porous flame arrester in combination with the used injector.

Following figure 1 during each test series, it was aimed to alter only one parameter while keeping the others constant during the test campaign. Thus the influence of only one single parameter could be investigated. The theoretical c^*_{theo} was calculated via NASA CEA [16] by using the reaction model "frozen at throat", this simulates an equilibrium reaction in the combustion chamber and a frozen flow downstream the nozzle throat. To derive c^*_{theo} the chamber pressure, mixture ratio and temperature data from the corresponding experiment were used as input parameters for NASA CEA. Furthermore, with the experimental results for the chamber pressure and the mass flow, c^*_{exp} was calculated according to equation 1. All c^* data shown in the diagrams below are based on the experimentally derived c^* values. By using the theoretical and experimental c^* values for the given test conditions, the combustion efficiency η_{c^*} was derived. Due to the premixed, gaseous state of the propellant, short characteristic chamber lengths (L^*) were expected.

A. Results of previous tests: influence of mixture ratio on c^*

In previous test campaigns [36, 37, 40] the occurring heat flux of the premixed N_2O/C_2H_4 propellant to the combustor's walls was studied in detail. It was found that the heat fluxes to the chamber walls are typically in the range of 0.5 $\frac{MW}{m^2}$ to 3.6 $\frac{MW}{m^2}$ and the heat loads are strongly depending on the chamber pressure, mixture ratio and chamber length. In addition, the influence of the oxidizer to fuel mixture ratio (ROF) on c^* was analysed [37]. The results of these previous campaign [37] are shown in figure 7. The diagram indicates the experimental data (black squares) and four different results for c^* depending on the assumed heat losses to the chamber walls for different chamber segment lengths. The grey line in figure 7 indicates the stoichiometric mixture ratio for N_2O and C_2H_4 at ROF=9.41.

The evaluation of these tests showed that heat losses to the chamber walls were the major factor influencing c^* and the combustion efficiency. The heat losses were modelled in CEA via reduction of the heat of formation of nitrous

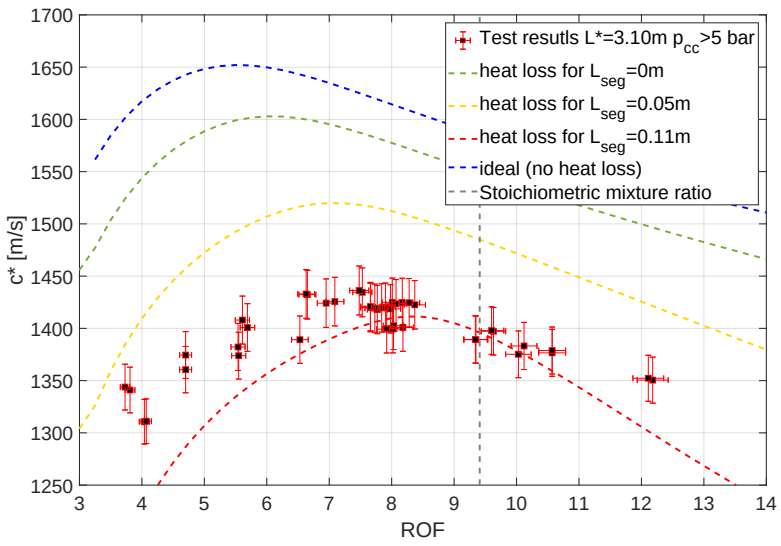

Fig. 7 c^* depending on ROF (oxidizer/fuel mass ratio) modified from [40]

oxide, a detailed description of the calculation procedure can be found in [40]. The mentioned process of reducing the propellant's inlet enthaply in CEA to account for heat losses was e.g. also used by Roth, Perakis and Haidn [41]. Due to the large L^* (3.10 m, $L_c c$= 0.1405 m) in this previous test series the combustion efficiency was only in between 74% and 92%. Detailed information about the test conduction, the results and the corresponding analysis can be found in [40]. Based on the results of the previous test campaign, the below described test series was started. The aim was to investigate the optimum L^*, to minimize heat losses and to raise the c^* efficiency. To avoid significant influences of the mixture ratio on c^*, the oxidizer to fuel ratio was kept in the range of 4.7 to 7.

B. Influence of L^* on c^* and η_{c^*}

Figure 8 and figure 9 show the obtained c^* and η_c^* for 134 conducted combustion tests. A wide variation of c^* values for a variation of the chamber length was found. This variation in c^* and η_c^* is caused by chamber pressure variations and slight deviations in the mixture ratio. The wide spread of the c^* values on the right hand side of diagram 8 (at L^* = 3.10 m) is caused by higher and lower values for the mass flow and mixture ratio for these tests compared to the other tests. So the mixture ratio ROF for the test with L^*=3.10 m was in between 3.5 and 12, while for all other chamber lengths the mixture ratio was kept in between 4.7 and 7. Especially the combination of a large L^* and a low chamber pressure resulted in a low c^*. Overall the variation of the mixture ratio and the mass flow results in a big variation of c^* and η_c^*.

The spread of c^* and η_c^* on the left hand side of figures 8 and 9(L^* approx. 0.5 m) is caused by pressure variations. A nearly identical L^* (see Table 2) could be achieved with a small nozzle throat and a shorter chamber or with a larger nozzle throat and a longer chamber. For identical mass flow, the use of a small nozzle throat will result in a higher chamber pressure, while the use of a larger nozzle throat will cause a lower chamber pressure.

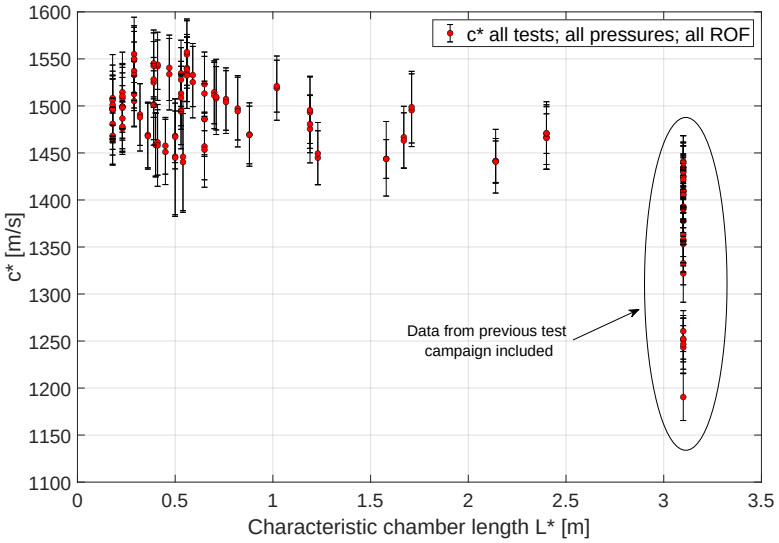

Fig. 8 c^* vs. L^* for all test runs

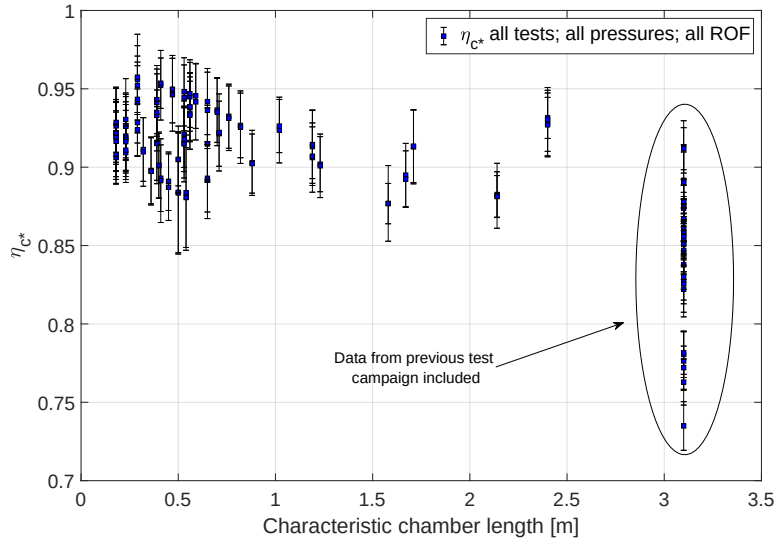

Fig. 9 η_c^* depending on L^* for all test runs

According to figure 1 four of five parameters which influence c^* should be kept constant. Otherwise the influence of the different parameters cannot be distinguished from each other and a clear analysis of the ideal combustion chamber size is not possible as figure 8 and figure 9 show.

C. Influence of chamber pressure p_{cc} on c^*

Due to the wide range of c^* and η_c^* shown in figure 9 and figure 9 the influence of the chamber pressure on c^* was investigated in detail. Figure 10 illustrates the influence of chamber pressure on c^* for a fixed chamber length (L_{cc} =

0.0305 m) and all used nozzle throat diameters (5 mm to 9 mm). For a specific nozzle throat diameter the chamber pressure was altered via in- or decrease of the propellant mass flow. The shown test results in figure 10 were obtained with the shortest possible chamber length. For this configuration the chamber surface was at a minimum and no chamber segment was mounted (see this configuration in figure 4b on the left). The black dotted line in figure 10 gives the theoretical values of c^*_{theo} calculated with CEA for a mixture ratio (ROF) of 7, 293 K and without a correction of the heat losses.

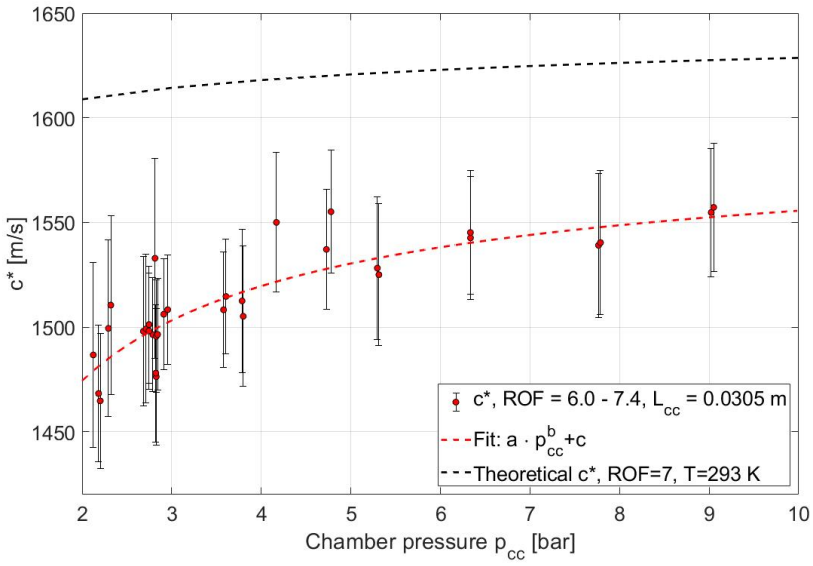

Fig. 10 Experimental c^* for a variation of the chamber pressure for a constant chamber length (L_{cc}) and for all nozzle throat diameters (5 to 9 mm)

Figure 10 indicates a clear influence of the chamber pressure on c^*. For pressures lower than 3 bar, c^* drops below 1500 m/s, while for pressures higher than 6 bar c^* is around 1550 m/s. Furthermore the influence of the pressure on c^* seems to decrease with higher pressure levels. With a higher chamber pressure the reaction speed increases and the combustion process approximates the ideal, infinite fast combustion process calculated by CEA. The shorter reaction time scales result in a rise of c^*. Furthermore the combustion temperature also slightly gets higher with increasing pressure, this also leads to a growth of c^*. Finally the released energy per volume also increases with rising chamber pressure. Figure 10 shows that the rise of additional energy caused by higher mass flow rates and the corresponding increase in chamber pressures exceeds the energy losses via heat conduction to the chamber walls. So with rising chamber pressure the heat generation due to the chemical reactions grows faster than the heat losses to the chamber walls increase. This correlation is also shown by conventional Nusselt correlations which are used to calculate the heat transfer coefficients and thus the heat flux in rocket engines (see e.g. [34, 42]). The Nusselt correlations generally show that an increase of the chamber pressure results in an increase of the heat flux, typically to the power of 0.8. So when the mass flow doubles, the chamber pressure also doubles, but the heat flux and thus the heat losses to the chamber

walls only increase by a factor of 1.74 ($2^{0.8}$). This means that with higher chamber pressures more kinetic energy for acceleration of the exhaust gases is available and the combustion efficiency increases.

D. Influence of L^* variation for constant chamber pressure on c^*

To investigate the influence of the characteristic chamber length L^* on c^*, the chamber pressure and mixture ratio had to be kept constant. The following two diagrams (figure 11 and figure 12) show c^* values for a small range of chamber pressure levels and mixture ratios. The test results shown in figure 11 and figure 12 were selected as the mixture ratio and the chamber pressure for each curve were in a very close range. During each test series the nozzle throat diameter (d_t) and the length of the chamber (L_{cc}) was varied.

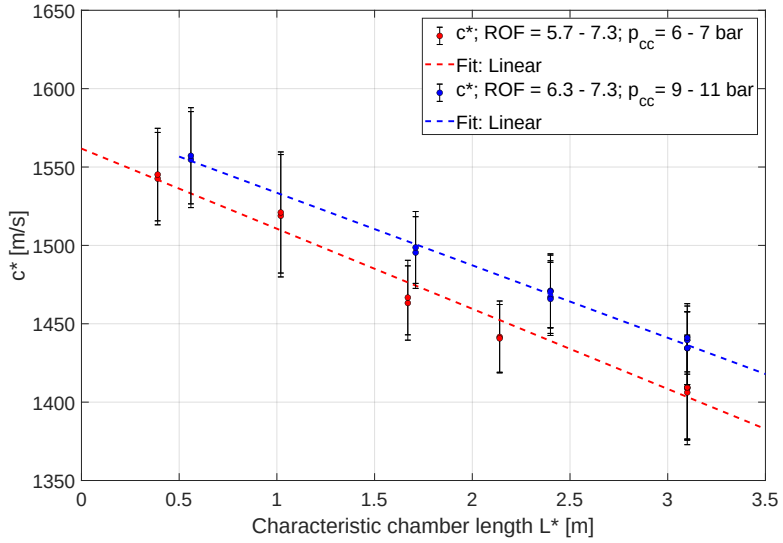

Fig. 11 Variation of L^* for mixture ratios in between 5.7 and 7.3 with chamber pressures between 6 and 7 bar as well as pressures in between 9 and 11 bar

For larger L^* values and higher pressure levels (figure 11), a nearly linear relationship in between L^* and the characteristic exhaust velocity was found. As mentioned in section IV.A and shown in [40], heat losses to the chamber walls are the main cause for a reduction of c^* and decrease of the corresponding combustion efficiency. The linear correlation of c^* with L^* seems to be reasonable: the characteristic chamber length L^* scales linear with the combustion chamber length (L_{cc} see equation 3) and also the chamber surface area scales linear with the combustion chamber length. So with a change in L^* the chamber surface area varies and this influences the energy loss to the chamber walls.

Figure 12 shows the resulting c^* for L^* values in between 0.23 m and 0.88 m. Due to boundary conditions of the setup, such as the supply pressure as well as the pressure drop of the injection and flashback arresting system, for large nozzle throat diameters the mass flow could not be increased arbitrarily. Thus, for large nozzle throats and corresponding low L^* values, the resulting chamber pressures were in between 3 to 4 bar. Caused by the lower pressure

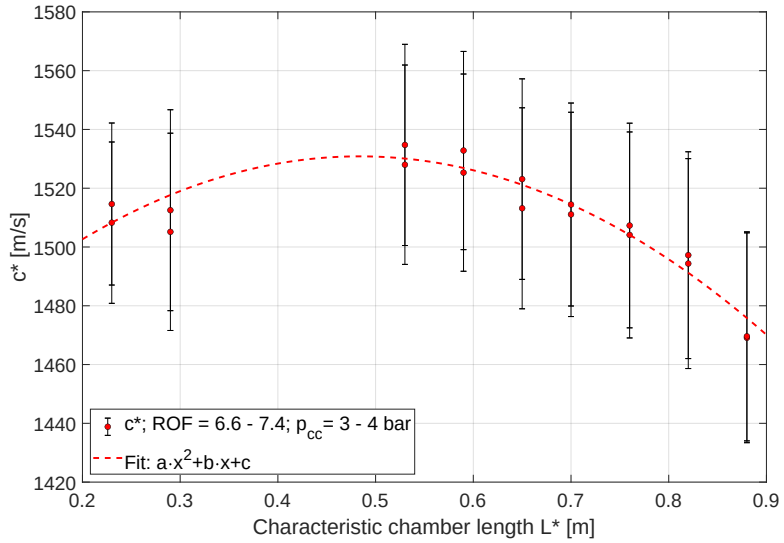

Fig. 12 Variation of L^* for mixture ratios in between 6.6 and 7.4 and chamber pressures between 3 and 4 bar

levels, the absolute c^* values are below the values for higher pressure levels (compare e.g. to figure 11). A quadratic fit was applied – showing a maximum of c^* for an L^* of approximately 0.5 m. The quadratic fit was chosen empirically and the authors will not state that a quadratic fit describes the underlying physics in a correct manner. After reaching a maximum at L^*= 0.5 m c^* drops again due to the increasing heat losses to the chamber walls of the capacitively cooled combustor. The optimum L^*_{opt} is comparable to high performance bipropellant combinations (e.g. the L^* for LOX/GH2 is 0.5-0.7 m [1, 43]). The small needed characteristic chamber length is most likely caused by the premixed, gaseous state of the propellant. No time is needed for atomization, evaporation or mixing of the components and the chemical time scales determines how short the combustion chamber can be. Typical injection speeds of the gaseous propellant are in the order of 20 m/s to 100 m/s, while the Reynolds numbers inside the injector bore holes are in the range of 30,000-100,000. As the atomization, evaporation and mixing is already finished, when the propellant enters the injection system, it is assumed that the used injector only has a very small influence on the optimum characteristic chamber length L^*_{opt}. Nevertheless, the used injection system will influence the optimum chamber length L^*_{opt}.

E. Combustion efficiency depending on Damköhler numbers: residence time (τ_{res}) and chemical time scale (τ_{chem})

As mentioned in paragraph II, L^* combines the effects of the propellants residence time in the combustor and the heat losses to the chamber walls. It is experimentally difficult to analyze both parameters independent from each other. Thus L^* should first show the effect of incomplete reactions – if the chamber or L^* is too small. Second a drop in efficiency for a large L^* should be visible, caused by excessive heat losses. Figure 12 shows both of these effects. To investigate the two effects more in detail, the chemical time scales (equation 7) and the flow time scales (equation 8)

for several tests runs were calculated and the corresponding Damköhler numbers were derived (equation 9). Here the calculation of the chemical time scale is based on the laminar flame speed S_L as the laminar flame speed is a characteristic parameter of a combustion process [44, 45]. As a turbulent flame can be interpreted as a folded and wrinkled laminar flame [45, 46], the laminar flame properties also describe the turbulent combustion process. Thus, the derived Damköhler number is also valid to describe turbulent combustion processes, as they take place inside the used rocket combustor. By using the Damköhler number, the variations of c^* with the mixture ratio and chamber pressure are taken into account and reduced to a single parameter.

$$\tau_{chem} = \frac{\alpha}{S_L^2} = \frac{\lambda}{\rho_u \, c_p \, S_L^2} \tag{7}$$

$$\tau_{res} = \frac{L_{cc} \, \rho_u \, A_{cc}}{\dot{m}} \tag{8}$$

To calculate the chemical time scale, the values for λ, ρ_u and c_p were taken from Refprop database [31], the laminar flame speed S_L was calculated via Cantera [47] using reaction mechanisms derived by Naumann et al. [30].
Figure 13 illustrates the resulting efficiencies for a wide variation of the Damköhler number.

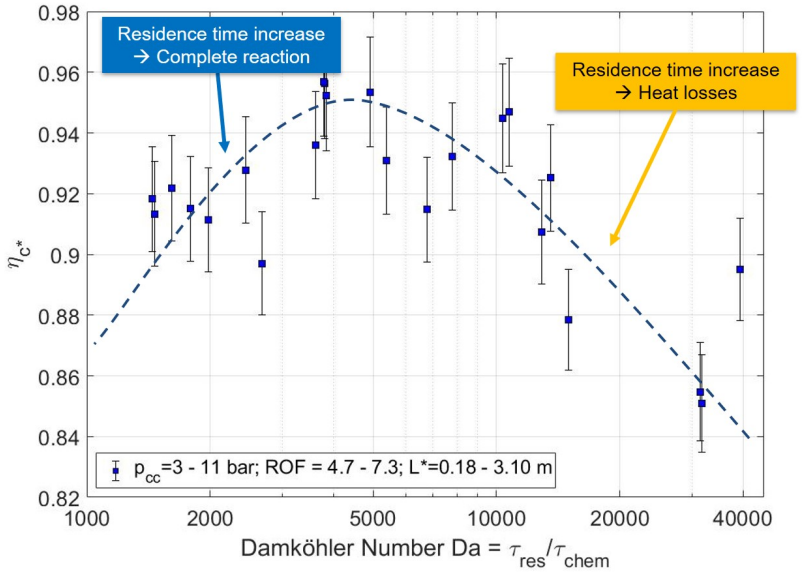

Fig. 13 Combustion efficiency depending on Damköhler number (residence time divided by chemical time scale) – Logarithmic scale of Da

Diagram 13 shows the c^* efficiencies depending on the calculated Damköhler numbers for chamber pressures in between 3 and 11 bar, for mixture ratios in between 4.7 and 7.3 and L^* values in between 0.18 m and 3.10 m. Two zones can be distinguished: A rise in efficiency with growing Da number until a maximum of Da = 4000 – 5000 is reached.

For higher residence times, the c^* efficiency drops significantly. Combining 1, 7 and 8 the following relationship is obtained:

$$Da = \frac{\tau_{res}}{\tau_{chem}} = \frac{L_{cc}\,\rho_u^2\,A_{cc}\,c_p\,c^*\,S_L^2}{p_{cc}\,A_t} \tag{9}$$

If the optimum Da number is known for the given injector, the combustion chamber can be designed efficiently. By knowing the optimum Da, a given diameter, an estimation of c^* and with the corresponding chamber pressure, the needed chamber length and contraction ratio can be calculated.

V. Conclusion

An extended test campaign with a premixed, green propellant consisting of nitrous oxide (N_2O) and ethene (C_2H_4) was carried out. The propellant called "HyNOx" – "hydrocarbons mixed with nitrous oxide" was used in gaseous state and burned in a capacitively (heat-sink) combustion chamber. The aim of the combustion tests was to investigate the influence of the mixture ratio (ROF), chamber pressure (p_{cc}) and the characteristic chamber length (L^*) on the combustors performance. The characteristic exhaust velocity c^* and the combustion efficiency η_c^* were taken into account to evaluate the influence of the mentioned parameters. The following parameters were varied during the campaign:

a) The mixture ratio. For a constant chamber geometry (L^* = 3.10 m, L_{cc} = 0.1405 m) the mixture ratio was varied. Large deviations from the theoretical performance were caused by extensive heat losses to the combustion chamber walls. During these tests the oxidizer to fuel mass ratio (ROF) with the highest c^* was found to be approximately 7 - while the stoichiometric composition of the propellant is given at a mixture ratio of 9.41 and the theoretical maximum of c^* without heat losses is located at ROF = 5.5.

b) The chamber pressure. For a fixed mixture ratio and a given, relatively short chamber length (L_{cc} = 0.0305 m) the pressure was raised via variation of the mass flow. The influence of the chamber pressure on the combustion efficiency is significant for pressure levels lower than 3 bar. For pressures higher than 6 bar, the influence of pressure on the performance decreases. Most likely the heat flux to the chamber walls causes this effect. The chamber pressure strongly influences the heat flux to the walls. For a rise of the chamber pressure, the additionally released energy inside the chamber exceeds the additional amount of energy conducted to the walls. Thus the heat losses do not rise as much as the chamber pressure increases – more energy is available to accelerate the hot combustion gases.

c) The characteristic chamber length L^*. L^* combines the effects of the chamber surface area (which causes heat losses) and the propellant residence time (which influences the completeness of the reaction). A maximum of c^* is obtained, if no excess heat is lost to the chamber walls and the reaction can take place completely. During the test campaigns, for the given injector and chamber design, an optimum L^* of about 0.5 m was found.

Furthermore a dimensionless Damköhler number (Da) was derived. To calculate the Da, the residence time of the unburned propellant in the combustion chamber was divided by the chemical time scale. By using the Damköhler number, the effects of mixture ratio and pressure variations during the test runs were reduced to a single parameter. For the used setup and propellant the maximum combustion efficiency was achieved at a Damköhler number of 4000 to 5000. Under these conditions a combustion efficiency of more than 95% and an absolute c^* of more than 1550 m/s was observed.

In the near future the authors plan to investigate nitrous oxide and a hydrocarbon in a conventional bipropellant system. Regarding the replacement of toxic MMH/NTO, the bipropellant use of N_2O and hydrocarbons may offer a safe, green and cheap alternative to the conventional, hypergolic mixture. The mentioned benefits (self-pressurization, good ignitability, good performance and no toxicity) could easily be utilized in a bipropellant system by avoiding the danger of a flame flashback.

Acknowledgments

The authors would like to thank the M11 test bench team: Hagen Friedrich, Ingo Dörr, Jan Buddenberg, and Konstantin Manassis for their help in preparing the test bench and the combustor. This work is funded by DLR's internal "Future Fuels" project. The support of DLR's Institute of Combustion Technology in Stuttgart is greatly acknowledged.

References

[1] Sutton, G. P., and Biblarz, O., *Rocket Propulsion Elements*, 8th ed., John Wiley & Sons and Wiley, Hoboken, N.J, 2010.

[2] Sackheim, R. L., and Masse, R. K., "Green Propulsion Advancement: Challenging the Maturity of Monopropellant Hydrazine," *Journal of Propulsion and Power*, Vol. 30, No. 2, 2014, pp. 265–276. https://doi.org/10.2514/1.b35086.

[3] Clark, J. D., *Ignition! An Informal History of Liquid Rocket Propellants*, Rutgers University Press classics, Vol. 2017: 1, Rutgers University Press and UMI Books on Demand, New Brunswick, N.J and Ann Abor, Mich., 2017.

[4] Persson, M., Anflo, K., and Friedhoff, P., "Flight Heritage of Ammonium Dinitramide (ADN) Based High Performance Green Propulsion (HPGP) Systems," *Propellants, Explosives, Pyrotechnics*, Vol. 44, No. 9, 2019, pp. 1073–1079. https://doi.org/10.1002/prep.201900248.

[5] Masse, R., Spores, and Allen, M., "Advanced Green Propulsion- GPIM and Beyond," *AIAA Propulsion and Energy 2020 Forum*, AIAA Paper 2020-3517, July 2020. https://doi.org/10.2514/6.2020-3517.

[6] Nosseir, A. E. S., Cervone, A., and Pasini, A., "Review of State-of-the-Art Green Monopropellants: For Propulsion Systems Analysts and Designers," *Aerospace*, Vol. 8, No. 1, 2021, p. 20. https://doi.org/10.3390/aerospace8010020.

[7] Negri, M., Wilhelm, M., and Ciezki, H., "Thermal Ignition of ADN-Based Propellants," *Propellants, Explosives, Pyrotechnics*, Vol. 44, No. 9, 2020, pp. 1096–1106. https://doi.org/10.1002/prep.201900154.

[8] Gohardani, A. S., Stanojev, J., Demairé, A., Anflo, K., Persson, M., Wingborg, N., and Nilsson, C., "Green space propulsion: Opportunities and prospects," *Progress in Aerospace Sciences*, Vol. 71, No. 1, 2014, pp. 128–149. https://doi.org/10.1016/j.paerosci.2014.08.001.

[9] Negri, M., Wilhelm, M., Hendrich, C., Wingborg, N., Gediminas, L., Adelöw, L., Maleix, C., Chabernaud, P., Brahmi, R., Beauchet, R., Batonneau, Y., Kappenstein, C., Koopmans, R.-J., Schuh, S., Bartok, T., Scharlemann, C., Gotzig, U., and Schwentenwein, M., "New technologies for ammonium dinitramide based monopropellant thrusters – The project RHEFORM," *Acta Astronautica*, Vol. 143, No. 1, 2018, pp. 105–117. https://doi.org/10.1016/j.actaastro.2017.11.016.

[10] Jankovsky, R. S., "HAN-Based Monopropellants Assessment for Spacecraft: NASA Technical Memorandum 107287: AIAA-96-2863," , 1996.

[11] Masse, R., Allen, M., Spores, R., and Driscoll, E. A., "AF-M315E Propulsion System Advances and Improvements," *52nd AIAA/SAE/ASME Joint Propulsion Conference*, AIAA Paper 2016-4577, July 2017. https://doi.org/10.2514/6.2016-4577.

[12] Hori, K., "Lessons Learned in the Thruster Tests of HAN," *Chemical Rocket Propulsion*, Springer Aerospace Technology, Springer International Publishing, Cham and s.l., 2017, pp. 801–818. https://doi.org/10.1007/978-3-319-27748-6_33.

[13] Amrousse, R., Katsumi, T., Azuma, N., and Hori, K., "Hydroxylammonium nitrate (HAN)-based green propellant as alternative energy resource for potential hydrazine substitution: From lab scale to pilot plant scale-up," *Combustion and Flame*, Vol. 176, No. 1, 2017, pp. 334–348. https://doi.org/10.1016/j.combustflame.2016.11.011.

[14] Katsumi, T., Inoue, T., Nakatsuka, J., Hasegawa, K., Kobayashi, K., Sawai, S., and Hori, K., "HAN-based green propellant, application, and its combustion mechanism," *Combustion, Explosion, and Shock Waves*, Vol. 48, No. 5, 2012, pp. 536–543. https://doi.org/10.1134/S001050821205005X.

[15] Wernimont, E. J., "System Trade Parameter Comparison of Monopropellants: Hydrogen Peroxide vs Hydrazine and Others," *42nd AIAA/ASME/SAE/ASEE Joint Propulsion Conference & Exhibit*, AIAA Paper 2006-5236, July 2006. https://doi.org/10.2514/6.2006-5236.

[16] McBride, B. J., and Gordan, S., "Computer Program for Calculation of Complex Chemical Equilibrium Compositions and Applications II. Users Manual and Program Description," NASA Reference Publication 1311, 1996. URL https://ntrs.nasa.gov/api/citations/19960044559/downloads/19960044559.pdf.

[17] Davis, D., Dee, L., Greene, B., Hornung, S., McCluer, M., and Rathgeber, K., "Fire, Explosion, Compatibility and Safety Hazards of Hydrogen Peroxide," NASA-TM-2004-213151, 2004. URL https://ntrs.nasa.gov/citations/20100040598.

[18] Ventura, M., Wernimont, E. J., Heister, S., Yuan, S., and Wernimont, E., "Rocket Grade Hydrogen Peroxide (RGHP) for use in Propulsion and Power Devices - Historical Discussion of Hazards," *43rd AIAA/ASME/AE/ASEE Joint Propulsion Conference and Exhibit*, AIAA Paper 2007-5468, 2007. https://doi.org/10.2514/6.2007-5468.

[19] Božić, O., Porrmann, D., Lancelle, D., and May, S., "Enhanced development of a catalyst chamber for the decomposition of up to 1.0 kg/s hydrogen peroxide," *CEAS Space Journal*, Vol. 8, No. 2, 2016, pp. 77–88. https://doi.org/10.1007/s12567-015-0109-x.

[20] Lauck, F., Balkenhohl, J., Negri, M., Freudenmann, D., and Schlechtriem, S., "Green Bipropellant Development – A Study on the Hypergolicity of Imidazole Thiocyanate Ionic Liquids with Hydrogen Peroxide in an Automated Drop Test Setup," *Combustion and Flame*, Vol. 226, 2021, pp. 87–97. https://doi.org/10.1016/j.combustflame.2020.11.033.

[21] Groot, W. A. d., Arrington, L. A., McElroy, J. F., Mitlitsky, F., Weisberg, A. H., Carter II, P. H., Myers, B., and Reed, B. D., "Electrolysis Propulsion for Spacecraft Applications," NASA Technical Memorandum 113157, AIAA-97-2948, 1997. URL https://ntrs.nasa.gov/archive/nasa/casi.ntrs.nasa.gov/19970041522.pdf.

[22] Harmansa, N.-E., Herdrich, G., Fasoulas, S., and Gotzig, U., "Development of a Satellite Propulsion System Based on Water Electrolysis," *International Journal of Energetic Materials and Chemical Propulsion*, Vol. 18, No. 3, 2019, pp. 185–199. https://doi.org/10.1615/IntJEnergeticMaterialsChemProp.2019028538.

[23] Reed, B. D., and Schneider, Steven, J., "Hydrogen Oxygen Auxiliary Propulsion Technology," AIAA Paper 91-3440. NASA-TM-105249, 1991. URL https://ntrs.nasa.gov/archive/nasa/casi.ntrs.nasa.gov/19920011280.pdf.

[24] Vozoff, M., and Mungas, G., "NOFBX™: A Non-Toxic, "Green" Propulsion Technology with High Performance and Low Cost," *53rd AIAA/SAE/ASEE Joint Propulsion Conference*, AIAA Paper 2012-5235, September 2012. https://doi.org/10.2514/6.2012-5235.

[25] Werling, L., Hörger, T., Manassis, K., Grimmeisen, D., Wilhelm, M., Erdmann, C., Ciezki, H., Schlechtriem, S., Richter, S., Methling, T., Goos, E., Janzer, C., Naumann, C., and Riedel, U., "Nitrous Oxide Fuels Blends: Research on premixed Monopropellants at the German Aerospace Center (DLR) since 2014," *AIAA Propulsion and Energy Forum*, AIAA Paper 2020-3807, August 2020. https://doi.org/10.2514/6.2020-3807.

[26] Werling, L., Jooß, Y., Wenzel, M., Ciezki, H. K., and Schlechtriem, S., "A premixed green propellant consisting of N_2O and C_2H_4: Experimental analysis of quenching diameters to desing flashback arresters," *International Journal of Energetic Materials and Chemical Propulsion*, Vol. 17, No. 3, 2018, pp. 241–262. https://doi.org/10.1615/IntJEnergeticMaterialsChemProp.2019027950.

[27] Werling, L., "Entwicklung und Erprobung von Flammensperren für einen vorgemischten, grünen Raketentreibstoff aus Lachgas (N2O) und Ethen (C2H4)," Dissertation, DLR-Forschungsbericht. DLR-FB-2020-39, 330 S, University of Stuttgart, Stuttgart, 2020.

[28] Gruss, M., "DARPA Scraps Plan To Launch Small Sats from F-15 Fighter Jet," , 30.11.2015. URL http://spacenews.com/darpa-airborne-launcher-effort-falters/.

[29] Werling, L., Lauck, F., Freudenmann, D., Röcke, N., Ciezki, H., and Schlechtriem, S., "Experimental Investigation of the Flame Propagation and Flashback Behavior of a Green Propellant Consisting of N2O and C2H4," *Journal of Energy and Power Engineering*, Vol. 11, No. 12, 2017, pp. 735–752. https://doi.org/10.17265/1934-8975/2017.12.001.

[30] Naumann, C., Kick, T., Methling, T., Braun-Unkhoff, M., and Riedel, U., "Ethene/Nitrous Oxide Mixtures as green Propellant to substitute Hydrazine: Reaction Mechanism validation," *International Journal of Energetic Materials and Chemical Propulsion*, Vol. 19, No. 1, 2020, pp. 65–71. https://doi.org/10.1615/IntJEnergeticMaterialsChemProp.2020028133.

[31] Lemmon, E. W., Bell, I. H., Huber, M. L., and McLinden, M. O., "NIST Reference Fluid Thermodynamic and Transport Properties Database: Version 9.1, NIST Standard Reference Database 23," , 2013. https://doi.org/10.18434/T4JS3C.

[32] Wilhelm, M., Negri, M., Ciezki, H., and Schlechtriem, S., "Preliminary tests on thermal ignition of ADN-based liquid monopropellants," *Acta Astronautica*, , No. 158, 2019, pp. 388–396. https://doi.org/10.1016/j.actaastro.2018.05.057.

[33] Turner, M. J. L., *Rocket and Spacecraft Propulsion: Principles, Practice and New Developments*, Springer, Berlin and Heidelberg, 2006.

[34] Bartz, D. R., "A Simple Equation for Rapid Estimation of Rocket Nozzle Convective Heat Transfer Coefficients: Technical Notes," *Journal of Jet Propulsion*, Vol. 27, No. 1, 1957, pp. 49–53. https://doi.org/10.2514/8.12572.

[35] Werling, L., Perakis, N., Hochheimer, B., Ciezki, H., and Schlechtriem, S., "Experimental Investigations based on a Demonstrator Unit to analyze the Combustion Process of a Nitrous Oxide/Ethene Premixed Green Bipropellant," *5th CEAS Air & Space Conference, 7.-11. September 2015, Delft, The Netherlands*, ????

[36] Perakis, N., Werling, L., Ciezki, H., and Schlechtriem, S., "Numerical Calculation of Heat Flux Profiles in a N2O/C2H4 Premixed Green Propellant Combustor using an Inverse Heat Conduction Method," *Space Propulsion Conference, 1.-5. May 2016, Rome, Italy*, 2016.

[37] Werling, L., Hörger, T., Ciezki, H. K., and Schlechtriem, S., "Experimental and Theoretical Analysis of the Combustion Efficiency and the Heat Loads on a N2O/C2H4 Green Propellant Combustion Chamber," *8th European Conference for Aeronautics and Space Sciences (EUCASS), 1.-4. July 2019, Madrid, Spain*, 2019. https://doi.org/10.13009/EUCASS2019-142.

[38] Bachmann, A., "Numerische Simulation der Strömung und Verbrennung in einem Green Propellant Raketentriebwerk," Bachelor thesis, Technical University Kaiserslautern, Kaiserslautern, 2021.

[39] DIN 1319-3, "DIN 1319-3:1996-05, Grundlagen der Meßtechnik_- Teil_3: Auswertung von Messungen einer einzelnen Meßgröße, Meßunsicherheit," , 1996-05-01. https://doi.org/10.31030/7204542.

[40] Werling, L., Hassler, M., Lauck, F., Ciezki, H. K., and Schlechtriem, S., "Experimental Performance Analysis (c* & c* Efficiency) of a Premixed Green Propellant consisting of N2O and C2H4," *53rd AIAA/SAE/ASEE Joint Propulsion Conference*, AIAA Paper 2017-5069, July 2017. https://doi.org/10.2514/6.2017-5069.

[41] Roth, C., Perakis, N., and Haidn, O. J., "Modeling Combustion and Heat Transfer in a Single-Element GCH4/GOX Rocket Combustor," *Proceedings of the 7th International Conference on Fluid Flow, Heat and Mass Transfer (FFHMT'20)*, Vol. Paper No. 178, 2020. https://doi.org/10.11159/ffhmt20.178.

[42] Gnielinski, V., "Neue Gleichungen für den Wärme- und den Stoffübergang in turbulent durchströmten Rohren und Kanälen," *Forschung im Ingenieurwesen A*, Vol. 41, No. 1, 1975, pp. 8–16. https://doi.org/10.1007/BF02559682, URL https://link.springer.com/article/10.1007/BF02559682.

[43] Messerschmid, E., and Fasoulas, S., *Raumfahrtsysteme: Eine Einführung mit Übungen und Lösungen*, 4th ed., Springer-Verlag Berlin Heidelberg, Berlin, Heidelberg, 2011. https://doi.org/10.1007/978-3-642-12817-2.

[44] Poinsot, T., and Veynante, D., *Theoretical and Numerical Combustion*, 3rd ed., CNRS, Paris, 2011.

[45] Glassman, I., Yetter, R. A., and Glumac, N. G., *Combustion*, fifth edition ed., Academic Press, Waltham, MA, 2015.

[46] Kuo, K. K., *Principles of Combustion*, 2nd ed., Wiley, Hoboken, NJ, 2005.

[47] David G. Goodwin, and Harry K. Moffat and Raymond L. Speth, "CANTERA: An object- oriented software toolkit for chemical kinetics, thermodynamics, and transport processes," , 2016. URL http://www.cantera.org/.